Applying a modified plane-wave expansion method to the calculations of transmittivity and reflectivity of a semi-infinite photonic crystal

Young-Chung Hsue
Department of Electrophysics, National Chiao-Tung University, Hsinchu, Taiwan, Republic of China and Department of Physics and Astronomy, Northwestern University, Evanston, Illinois 60201, USA

Tzong-Jer Yang
Department of Electrophysics, National Chiao-Tung University, Hsinchu, Taiwan, Republic of China
(Received 30 July 2003; revised manuscript received 2 February 2004; published 26 July 2004)

We propose a modified plane-wave expansion method to calculate transmittivity and reflectivity of a semi-infinite photonic crystal (PC) with interface. This method is based on an expanded completeness basis, including both the propagation and evanescence modes. We use this approach to deal with two kinds of problems: one is to determine the normal direction of the largest attenuation strength for a semi-infinite PC in the gap frequencies; the other is to calculate the transmittivity and reflectivity of a PC slab. To demonstrate the extensive utilization of our approach, we revisit the same system as studied by K. Sakoda [Phys. Rev. B **52**, 8992 (1995)] and find that our results are in good agreement with ones obtained by Sakoda's paper.

DOI: 10.1103/PhysRevE.70.016706 PACS number(s): 02.70.−c, 42.70.Qs, 85.60.Bt

Since Yablonovitch and John [1–3] proposed the concept of the photonic crystals (PC's), the studies of the properties of the PC's and their fabrications have attracted great interest. PC's are of artificial materials having the periodical modulation of dielectric function in space and there exist photonic band gap (PBG) structures for electromagnetic (EM) waves. Many novel features of PC's have been predicted and a lot of potential applications are suggested [4–6]. Most of the studies focus on the PBG structures with the use of the conventional plane-wave expanded method (PWEM) [7,8]. Subsequently, various calculation methods are presented to investigate physical properties, such as the transmission, reflection, and the penetration depth of the incident EM waves through the finite-sized PC's [9–12].

Motivated by these works, we now present a different calculation method to ease the calculations of the transmission, reflection, and wave penetration depth for finite-sized PC's with interfaces or surface. Our approach is a natural generalization of the original PWEM and it is based on an expanded basis, including both the propagation modes and the evanescence modes in the PC's. Our approach possesses several advantages: First, it makes it easier to flexibly track and analyze the properties of the PC's; second, in our method the frequency is initially given and regarded as a known variable, rather than an argument, thus the value of frequency can be always set to be positive real even for the complex systems with real (imaginary, or complex) frequency-dependent permittivity or permeability; third, the resonant feature of transmittivity generated from the finite size of the PC's can be easily analyzed. We numerically demonstrate that our approach has a more powerful and efficient method to track the above-addressed problems, compared to the conventional PWEM.

In an isotropic medium with spatial modulated permittivity $\epsilon(\mathbf{r})$ and permeability $\mu(\mathbf{r})$, according to Maxwell equations, the magnetic field $\mathbf{H}(\mathbf{r})$ satisfies

$$\nabla \times \frac{1}{\epsilon(\mathbf{r})} \nabla \times \mathbf{H}_\omega(\mathbf{r}) = \mu(\mathbf{r})\omega^2 \mathbf{H}_\omega(\mathbf{r}). \tag{1}$$

As $\epsilon(\mathbf{r})$ and $\mu(\mathbf{r})$ are periodical modulation functions in the PC's, we can then expand them and the magnetic field in terms of Fourier series as $\mathbf{H}_\omega(\mathbf{r}) = \sum_{\mathbf{G}} e^{i(\mathbf{k}+\mathbf{G})\cdot\mathbf{r}} \mathbf{H}_{\mathbf{k},\mathbf{G}}$; $\epsilon(\mathbf{r}) = \sum_{\mathbf{G}} e^{i\mathbf{G}\cdot\mathbf{r}} \epsilon_{\mathbf{G}}$; and $\mu(\mathbf{r}) = \sum_{\mathbf{G}} e^{i\mathbf{G}r} \mu_{\mathbf{G}}$. Here $\{\mathbf{G}\}$ denotes the reciprocal lattice vector. Equation (1) can then be rewritten as

$$-\sum_{\mathbf{G}'} (\mathbf{k}+\mathbf{G}) \times \epsilon^{-1}_{\mathbf{G}-\mathbf{G}'}(\mathbf{k}+\mathbf{G}') \times \mathbf{H}_{\mathbf{k},\mathbf{G}'} = \omega^2 \sum_{\mathbf{G}'} \mu_{\mathbf{G}-\mathbf{G}'} \mathbf{H}_{\mathbf{k},\mathbf{G}'}. \tag{2}$$

In two-dimensional (2D) systems, the electromagnetic wave equation (2) can be decoupled to two separate equations for the *E* polarization (TE) (in-pane electric field) and *H* polarization (TM) (in-plane magnetic field) modes:

$$\sum_{\mathbf{G}'} \epsilon^{-1}_{\mathbf{G}-\mathbf{G}'}(\mathbf{k}+\mathbf{G}) \cdot (\mathbf{k}+\mathbf{G}') H_{\mathbf{k},\mathbf{G}'} = \omega^2 \sum_{\mathbf{G}'} \mu_{\mathbf{G}-\mathbf{G}'} H_{\mathbf{k},\mathbf{G}'} \tag{3}$$

for the TM modes.

Apparently, Eq. (3) belongs to a standard eigenvalue equation when the permittivity and permeability are real and frequency independent. In an infinite extended periodic system, the frequencies of the propagating modes for a given real $\mathbf{k}$ can be obtained straightforwardly. However, in a PC slab or semi-infinite PC, the calculations of the transmission and reflection of the EM waves are not simple. Various calculation methods such as the Layer-Korringa-Kohn-Rostoker (LKKR) method [8,9,11], the transfer matrix method [12–15], and the scattering matrix method [16–18] have been proposed.

We propose an alternative method to calculate the transmitted and reflected wave fields for a PC slab. This method still relies upon Eq. (3), but we employ an alternative view angle to deal with this equation, different from the standard eigenequation method. To clearly look at the central point of this method, we revisit the standard eigenequation method in some detail. At the beginning, the k_x and k_y are initially chosen in the first Brillouin zone as the known parameters, and the eigenfrequency ω can thus be determined through solving a standard eigenequation. For the infinitely extended system, there exist only propagation modes, however, for a PC slab or semi-infinite system, there exists at least one interface. At interfaces, the periodicity of structure is broken and the evanescent modes are generated. Using the conventional eigenequation method Eq. (3) it is quite difficult to find the evanescent modes because it belongs to a search for the real eigenfrequency solution but with a complex number of k. In general, the complex ω is the result of Eq. (3) when k is an arbitrary complex number. However, the complex ω is unacceptable or unavailable. Consequently, one natural and important question arises: Can we have a new solving method to automatically obtain the evanescence modes of Eq. (3)? The answer is positive. For different goals, there are two kinds of the calculated schemes: One is that from initially choosing the unit vectorial direction of $\mathbf{k}$ and a given frequency, one then searches for the solution to Eq. (3); the second scheme is when initially given k_y and frequency, one then searches for the solution to Eq. (3). We now discuss them in detail. For the first scheme, we reform Eq. (3) as

$$\begin{pmatrix} 0 & \hat{\mathbf{I}} \\ \epsilon_{\mathbf{G}-\mathbf{G}''}[\omega^2\mu_{\mathbf{G}''-\mathbf{G}'} - \epsilon^{-1}_{\mathbf{G}''-\mathbf{G}'}\mathbf{G}''\cdot\mathbf{G}'] & -\epsilon_{\mathbf{G}-\mathbf{G}''}[\epsilon^{-1}_{\mathbf{G}''-\mathbf{G}'}\hat{\mathbf{k}}\cdot(\mathbf{G}''+\mathbf{G}')] \end{pmatrix}\begin{pmatrix} H_{\mathbf{G}'} \\ kH_{\mathbf{G}'} \end{pmatrix} = k\begin{pmatrix} H_{\mathbf{G}'} \\ kH_{\mathbf{G}'} \end{pmatrix}, \tag{4}$$

where $H_{\mathbf{G}'}$, $\hat{\mathbf{I}}$, and $\hat{\mathbf{k}}$ denote the abbreviation of $H_{\mathbf{k},\mathbf{G}'}$, $\delta_{\mathbf{G},\mathbf{G}'}$, and unit vector of $\mathbf{k}$, respectively. Regarding the second scheme, Eq. (3) can be rewritten in another form as

$$\begin{pmatrix} 0 & \hat{\mathbf{I}} \\ \epsilon_{\mathbf{G}-\mathbf{G}''}[\omega^2\mu_{\mathbf{G}''-\mathbf{G}'} - \epsilon^{-1}_{\mathbf{G}''-\mathbf{G}'}(\mathbf{G}''+k_y\hat{\mathbf{y}})\cdot(\mathbf{G}'+k_y\hat{\mathbf{y}})] & \hat{\mathbf{P}} \end{pmatrix} \times\begin{pmatrix} H_{\mathbf{G}'} \\ k_xH_{\mathbf{G}'} \end{pmatrix} = k_x\begin{pmatrix} H_{\mathbf{G}'} \\ k_xH_{\mathbf{G}'} \end{pmatrix}, \tag{5}$$

where $\hat{\mathbf{y}}$ denotes the unit vector of the y direction and $\hat{\mathbf{P}} = -\epsilon_{\mathbf{G}-\mathbf{G}''}[\epsilon^{-1}_{\mathbf{G}''-\mathbf{G}'}(\mathbf{G}''_x+\mathbf{G}'_x)]$. It is worth pointing out an important fact that in these equations, we have extended the original basis of $\{H_{\mathbf{G}'}\}$ to an expanded basis of $\{(H_{\mathbf{G}'}, kH_{\mathbf{G}'})\}$. The matrix on the left side of Eq. (4) no longer presets Hermitianity now. Therefore Eq. (4) belongs to the pseudoeigenvalue problem with complex number of k. The eigenfunctions of the expanded basis contain the propagation and evanescence modes both. The modes having the complex k correspond to oscillatory decay or growing modes. All these modes can be automatically obtained by using this approach. It is noted that there exists a simple transform between these two equations: If $\mathbf{k}$ and $\mathbf{G}$ in Eq. (4) are taken on a rotation operator $\hat{\Theta}$, i.e., rotating $\hat{\mathbf{k}}$ to be parallel to the x direction, $\hat{\Theta}\hat{\mathbf{k}}=\hat{\mathbf{x}}$, and we define $\tilde{\mathbf{G}}\equiv\hat{\Theta}\mathbf{G}$, then Eq. (4) will transform to Eq. (5) except for the replacement of $\mathbf{G}$ by $\tilde{\mathbf{G}}$ and $k_y=0$. In this sense, Eq. (4) can be referred to as a master equation. Through solving this master equation, the penetration depth of the incident waves along direction $\hat{\mathbf{k}}$ can be easily evaluated.

On the other hand, Eq. (5) can be used to deal with the incline incident case with an incident angle θ between the normal of the interface and $\mathbf{k}$. Here we define $\tan\theta = k_y/\sqrt{(\omega/c)^2-k_y^2}$. Employing a matching technique, the relationship between the $\mathbf{H}$ fields in region I and region II can be established,

$$\begin{pmatrix} -\langle x_0y|H^{\mathrm{I}}_m\rangle & \langle x_0y|H^{\mathrm{II}}_m\rangle \\ -\langle x_0y|\epsilon^{-1}\partial_x|H^{\mathrm{I}}_m\rangle & \langle x_0y|\epsilon^{-1}\partial_x|H^{\mathrm{II}}_m\rangle \end{pmatrix}\begin{pmatrix} \langle H^{\mathrm{I}}_m|\hat{\mathbf{r}}|H^{\mathrm{I}}_0\rangle \\ \langle H^{\mathrm{II}}_m|\hat{\mathbf{t}}|H^{\mathrm{I}}_0\rangle \end{pmatrix} = \begin{pmatrix} \langle x_0y|H^{\mathrm{I}}_0\rangle \\ \langle x_0y|\epsilon^{-1}\partial_x|H^{\mathrm{I}}_0\rangle \end{pmatrix}, \tag{6}$$

where $\hat{\mathbf{r}}$ and $\hat{\mathbf{t}}$ represent the reflection and transmission operators. $H^{\mathrm{I}}_m(H^{\mathrm{II}}_m)$ corresponds to the mth reflected (transmitted) mode in region I (II), and H^{I}_0 to the incident field (see Fig. 1).

Theoretically, as long as we obtain overall eigenvectors of the system, the transmission and reflection spectra can then be determined fully. However, for a semi-infinite PC, we only need the special modes with the parallel wave vector component k_y identical to that of incident light wave owing to the conservation of the k_y in either sides of interface. We now assume that the wave vector of the incident light is $\mathbf{k}=(k_x^{\mathrm{I},i},k_y)$, according to the Bloch theory, the magnetic field in region II can be expressed as $H(\mathbf{r})=\Sigma_{\mathbf{G}}H_{\mathbf{G}}\exp[i(\mathbf{k}^{\mathrm{II},t}+\mathbf{G})\cdot\mathbf{r}]$, where G denotes the reciprocal vector. By using the matching technique, for the reflection modes and transmission modes, their wave vectors should be $\mathbf{k}_{ref}=(k_x^{\mathrm{I},r},k_y+G_y)$ and $\mathbf{k}_{trans}=(k_x^{\mathrm{II},t}+G_x,k_y+G_y)$, where $k_x^{\mathrm{I},r}=-\sqrt{(\omega/c)^2-(k_y+G_y)^2}$, and $k_x^{\mathrm{II},t}$'s are obtained from solving Eq. (5). Hence, in the k space, Eq. (6) can be expressed as

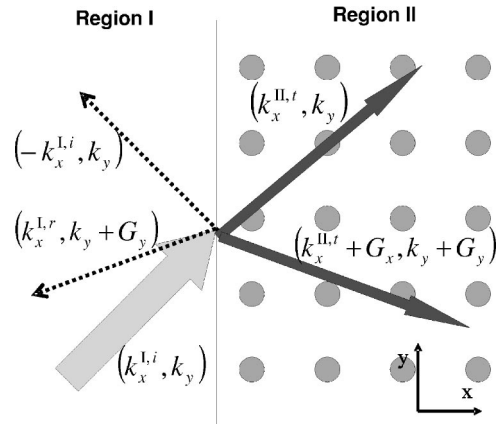

FIG. 1. Schematic view of the system used in this paper. The system is composed of a semi-infinite PC (referred to as Region II), positioned at the *xy* plane, embedded in a vacuum (referred to as Region I). The gray, dotted, and black arrows indicate the directions of the wave vectors for the incident, reflected, and transmitted waves, respectively. The superscripts *i*, *r*, and *t* denote the incident, reflective, and transmitted fields, respectively.

$$\hat{\mathbf{A}}\begin{pmatrix} \langle H_m^{\mathrm{I}}|\hat{\mathbf{r}}|H_{10}\rangle \\ \langle H_m^{\mathrm{II}}|\hat{\mathbf{t}}|H_{10}\rangle \end{pmatrix} = \begin{pmatrix} H_{G_y,0}^{\mathrm{I},i} \\ k_{G_y,x}^{\mathrm{I},i} H_{G_y,0}^{\mathrm{I},i} \end{pmatrix}, \tag{7}$$

where

$$\hat{\mathbf{A}} = \begin{pmatrix} -H_{G_y,m}^{\mathrm{I},r} & \sum_{G_x} H_{\mathbf{G},m}^{\mathrm{II},t} \\ -k_{mx}^{\mathrm{I},r} H_{G_y,m}^{\mathrm{I},r} & \sum_{G_x,\mathbf{G}'} \epsilon_0 \epsilon_{\mathbf{G}-\mathbf{G}'}^{-1} (k_{mx}^{\mathrm{II},t} + G_x') H_{\mathbf{G},m}^{\mathrm{II},t} \end{pmatrix},$$

ϵ_0 is the dielectric constant of vacuum and $H_{\mathbf{G},m}$ is the *m*th mode obtained from the solution to Eq. (5). Regarding the eigenvectors in region I (for instance, in vacuum), they are of plane waves, only depending on G_y, so their Fourier components are abbreviated as $H_{G_y,m}$ instead of $H_{\mathbf{G},m}$. To evaluate the transmission and reflection coefficients, we have to first decide the direction of the Poynting vector of every mode. When $\mathbf{k}$ is real, it can either be obtained from $\mathbf{v}_g = \nabla_{\mathbf{k}}\omega$ or from

$$\mathbf{v}_g = \int_{cell} \mathrm{Re}\left\{ -\frac{i}{\omega\epsilon} H^* \nabla H \right\} dr^2$$

$$= \sum_{\mathbf{G},\mathbf{G}'} \mathrm{Re}\left\{ \frac{1}{\omega} H_{\mathbf{k},\mathbf{G}}^* \epsilon_{\mathbf{G}-\mathbf{G}'}^{-1} (\mathbf{k} + \mathbf{G}') H_{\mathbf{k},\mathbf{G}'} \right\}. \tag{8}$$

However, when $\mathbf{k}$ is complex, from the physical consideration, the right-forward propagation mode should correspond to $\mathrm{Im}(k_x) > 0$. When the group velocity and $H_{\mathbf{G}}$ of each mode are known, the transmittance *T* and reflectance *R* can be calculated from them and the accuracy is estimated from the derivation degree of $R+T$ from unity. Sometimes, it is possible that $\det|\mathbf{A}|$ approaches zero, if so, it demands that Eq. (7) has nonzero solutions in the absence of the incident light field. This kind of wave fields corresponds to surface states,

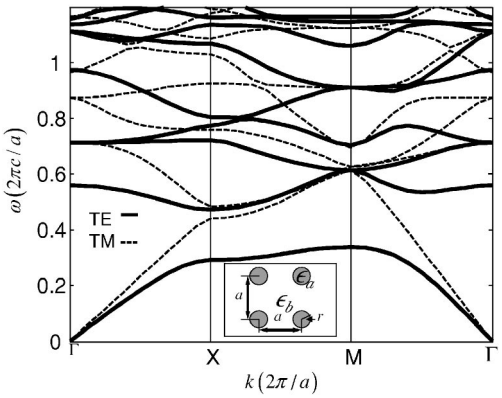

FIG. 2. Calculated frequency dispersion spectrum of a 2D PC by Eq. (2). The sample is composed of a square lattice of GaAs dielectric circular cylinders with $r=0.15a$ and $\epsilon/\epsilon_0=11.43$ in air. The solid and dashed curves represent the TE and TM modes, respectively. The inset shows the unit cell of the PC.

i.e., the counterpart of surface plasmons propagating along the surface of a metal.

It is worth emphasizing that there exists more interesting matter among these three equations, Eqs. (3)–(5): they can be intertransformed with each other. For instance, the second line of matrices on the left-hand side of Eqs. (4) and (5) just is identical to Eq. (3) when fixed $\{\mathbf{G}\}$. Thus any eigenfunction derived from one of these three equations will satisfy the other two equations. It leads to two useful conclusions: (i) the contours of real $\mathbf{k}$ obtained by these three equations exhibit the same patterns; (ii) the choice of the set of $\{\mathbf{G}\}$ does not require any change when employing these three equations to track different problems. For instance, when seeing what happens near the band gap, we first need to find where the band edges are located by solving Eq. (3) and then substitute a frequency ω_0 near the band edges into Eqs. (4) and (5), the penetration depth of the incident wave into the interface of sample can then be computed by Eq. (4). Similarly, the transmittivity can be calculated if we first solve Eq. (5) and then substitute the obtained quantities into Eq. (6).

We now turn to demonstrate the utilizations of our approach via some examples. Figure 2 displays the calculated frequency dispersion spectrum of the 2D PC by Eq. (2). The sample is composed of a square lattice of GaAs dielectric circular cylinders with $r=0.15a$ and $\epsilon/\epsilon_0=11.43$ in air. The solid and dashed curves represent the TE and TM modes, respectively. The inset shows the unit cell of the PC.

For another application example, we investigate the guidance rule to decide the favorable normal direction of the incident light waves at interface of a semi-infinite PC sample for supporting the function of the most isolating of the light wave fields in the sample. We solve Eq. (4) at a given frequency of $0.4(2\pi c/a)$ around the mid gap of the TE modes (see Fig. 2). Figure 3 displays the distribution of possible $\mathbf{k}$ for this given frequency. The solid square frames indicate the first Brillouin zone boundaries and all data available should be located at interior of this zone. (a) and (b) correspond to the TM modes (*H* polarization); (c) and (d) correspond to the TE modes (*E* polarization). (a) and (c) display the equifrequency contours for the TM and TE modes, respectively,

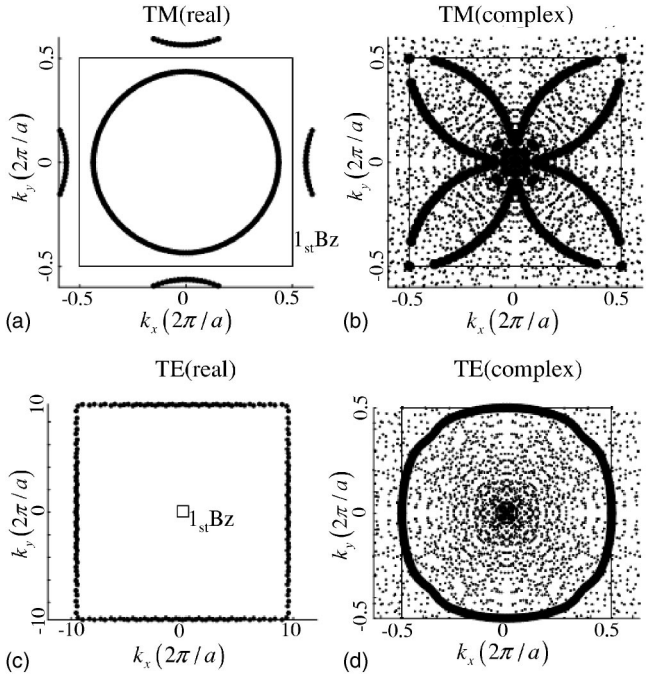

FIG. 3. Distribution of possible **k** values for a given frequency $\omega=0.4(2\pi c/a)$. The parameters of this system are the same as those of Fig. 2. The solid square frames indicate the first Brillouin zone boundaries and all the data available should be located at interior of this zone. (a) and (b) correspond to the TM modes (*H* polarization); (c) and (d) correspond to the TE modes (*E* polarization). (a) and (c) display the equifrequency contours for the TM and TE modes, respectively, when **k** of propagating waves takes pure real number. Similarly, (b) and (d) show the contours of Re{**k**} for the TM and TE evanescent modes with complex **k**. The spots in (b) and (d) correspond to the situations with the smallest Im(**k**) or longest penetration depth.

when **k** of propagating waves takes pure real number. Similarly, (b) and (d) show the contours of Re{**k**} for the TM and TE evanescent modes with complex **k**. The spots in (b) and (d) correspond to the situations with the smallest Im[$\mathbf{k}(\theta)$] or longest penetration depth. It is clearly seen from Fig. 3(c) that there are not any real number solutions of **k** inside the first Brillouin zone due to the fact that the given frequency $\omega=0.4(2\pi c/a)$ is located at the mid gap of the TE modes. However, when **k** is allowed to expand outside or far away from the first Brillouin zone, thus the solution of the real number **k** for this same frequency can be found. Such solutions are missed owing to the finite number of the basis used in the calculations. To find the interfacial direction in which the penetration depth has the largest value, we first fix a direction $\hat{\mathbf{k}}$ and use Eq. (4) to find a wave vector of k that corresponds to the smallest $|\mathrm{Im}(k)|$ value, denoted as $k_I(\theta)$, and it decides the primal decay trend for a propagating wave along $\hat{\mathbf{k}}$. The second step is to scan the incident angle of θ from 0° to 45° (if the considered system has a symmetry lower than the present discussed sample, the scanning range of the angle should be extended from 0° to 180°) to find an angle θ_0, corresponding to the maximum $k_I(\theta)$. The contour of minimum value of imaginary part of k of the TE modes

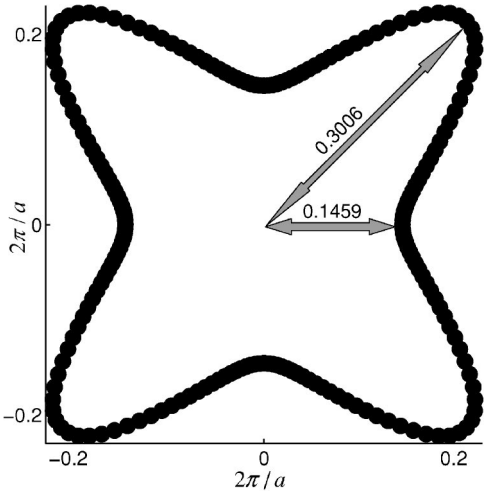

FIG. 4. Contour of minimum value of imaginary part of k of the TE modes for each given incident angle θ, denoted by $k_I(\theta)$. $k_I(0°)$ and $k_I(45°)$ are 0.1459 and 0.3006, respectively. The real part of k is shown by spots in Fig. 3(d).

for every given incident angle θ, denoted as $k_I(\theta)$, is shown in Fig. 4. The penetration depths, defined by $2\pi/k_I(\theta)$, are $6.8540a$ and $3.3272a$ at the incident angle of 0° and 45°, respectively. This implies that when cutting a sample along 45°, it just needs four or five layers, enough to sufficiently block the incident light waves with $\omega=0.4(2\pi c/a)$ and TE polarization through the sample at all, instead of seven or eight layers needed for the 0°-cut sample.

The second example is that fixed k_y and frequency, one searches for the k_x satisfied Eq. (5), and then computes the transmittivity. For providing a better comparison, we consider a similar sample discussed in Ref. [9]. The sample is a 16-layer PC slab; the PC consists of a square lattice of air circular rods with a radius of $0.43077a$ (a is the lattice constant) in the dielectric PbO material ($\epsilon=2.72\epsilon_0$). The transmission spectrum of this sample can be calculated by Eqs. (5) and (7), as shown in Fig. 5, for two polarizations: (a) for TE and (b) for TM modes. The curves with dots are drawn by data excerpted from Ref. [9]. The solid and dashed curves correspond to our results (our sample corresponds to a semi-infinite PC, rather than a PC slab) for two different manners of cutting plane as making the surface of the semi-infinite PC sample: The solid curve that corresponds to the cutting plane is the same as that in Ref. [9], whereas the dashed curve corresponds to another manner of cutting plane which just passes through the central line of hole rods at the surface layer. The inset shows a magnified plot of (a) in part for a clearer view of (a). The frequency regime now is settled from 0.72 to 0.85, indicated by ↔.

Our sample is semi-infinite in space therefore our results are significantly different from those obtained by Sokoda [9]. The main difference is summarized below.

(i) It is clearly seen that the solid and dashed curves almost exhibit smooth varying behavior except for some parts near the gap regime and at some special frequencies, for instance, at $\omega=0.74$ and 0.85 in the TE mode. However, the solid curves with dots correspond to the Sakoda's results in Ref. [9], they exhibit strongly oscillatory behavior owing to

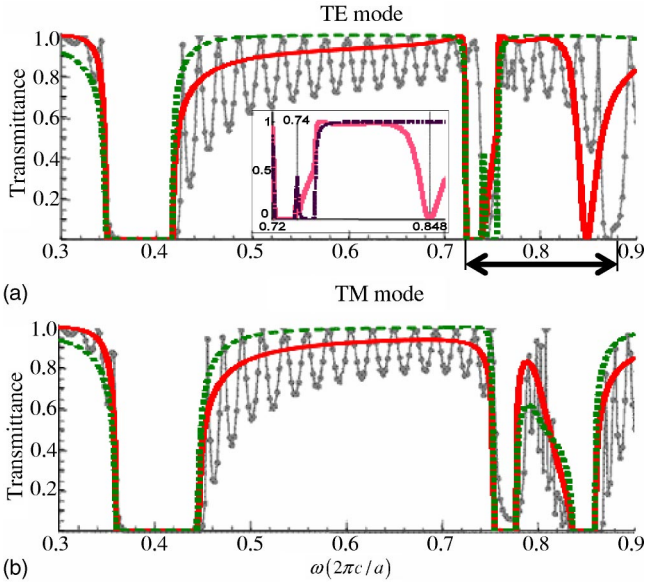

FIG. 5. Transmittance spectrum of a semi-infinite PC in air for two polarization states of the incident light: (a) for TE and (b) for TM modes. The related parameters of the sample have been described in the text. The curves with dots are drawn by the data excerpted from Ref. [9]. The solid and dashed curves correspond to our results for two different manners of cutting plane to form the semi-infinite PC sample: the solid curve to the cutting plane being the same as that in Ref. [9] and shown in Fig. 2, whereas the dashed curve to another cutting manner of the surface of our sample, the surface is cut through the central line of hole rods of the first layer. The inset displays a magnified plot of (a) in part, whose frequency regime is indicated by a ↔.

the finite thickness of his sample. This oscillation structure can be interpreted by a rough argument with the use of the average dielectric constant, given by $\bar{\epsilon} \equiv \langle \epsilon \rangle_{cell}$. In the low frequency regime, the most important contribution to $\epsilon_{\mathbf{G}}$ comes from the terms of $\epsilon_{\mathbf{G}=0}$ (i.e., $\bar{\epsilon}$) in the series expansion. Thus a 16-layer PC slab can be treated as a single dielectric plate with an effective uniform dielectric constant $\bar{\epsilon} = 1.7173\epsilon_0$ and a width of $16a$, surrounded by air. This is a typical 1D problem and the fields in both sides of this plate are connected by a transfer matrix as

$$\mathbf{M}_\omega \begin{pmatrix} e^{ik16a} & 0 \\ 0 & e^{-ik16a} \end{pmatrix} \mathbf{M}_\omega^{-1},$$

where $\mathbf{M}_\omega$ represents a 2×2 matrix with $\det|\mathbf{M}_\omega| \neq 0$, dependent on the optical impedance contrast and the incident angle. $k = \omega\sqrt{\bar{\epsilon}\mu_0}$ is the effective wave number, μ_0 is permeability in free space. It is evident that the middle propagating matrix equals $\pm\mathbf{I}$ when $k16a = n\pi$, where n is an integer number, so does the total transfer matrix. This manifests that the frequency spacing between two neighboring peaks is

$$\Delta\tilde{\omega} = \frac{1}{32\sqrt{\bar{\epsilon}/\epsilon_0}} = \frac{1}{32\sqrt{1.7173}} \simeq 0.0238,$$

where $\tilde{\omega} = \omega(a/2\pi c)$. We find that the average spacing of two consecutive peaks in Fig. 5 is 0.0222 over the range of $\tilde{\omega} = [0.5, 0.7]$ therefore we can safely conclude that the oscillations in Fig. 5 come definitely from the effect of finite thickness of the sample.

(ii) In the vicinity of $\tilde{\omega} \simeq 0.74$, the transmittivity is expected to be ascended rapidly with the increase of $\tilde{\omega}$ because this frequency approaches the expanded band edge. However, the realistic situation exhibits different varying behavior; see the inset of Fig. 5(a). The transmittivity at the beginning ascended quickly and subsequently it drops rapidly to zero. This phenomenon can be interpreted by the fact that there are two propagation modes with near zero group velocity ($v_g \simeq 0$), consequently, they make small contribution to the transmittivity.

(iii) It is clearly seen from the inset of Fig. 5(a) that the valley of transmittivity near $\tilde{\omega} = 0.85$ disappears when the surface is located at the central line of hole rods of the first layer, different from the solid curve, corresponding to the surface cut along the middle plane between two adjacent hole rod layers. This result implies that it is possible to block the incident light waves at some discrete frequencies by appropriately choosing the cutting plane to serve as the surface of the semi-infinite PC sample even the frequencies of the incident light waves fall out off the photonic band gaps.

(iv) It is observed from Fig. 5(b) that there should exist a forbidden band for $\tilde{\omega} = 0.75$ to 0.78; see the solid curve. However, the curve with dots never does show this merit. According to our calculations, the attenuation rate of the incident fields for a 16-layer PC slab sample is about 0.0733, which agrees with the result shown in the dots curve. This infers an important conclusion that evanescence modes indeed offer the contribution to the transmittivity in a finite thickness PC slab.

We now conclude that the evanescence modes play a critical role and they should be taken into account in the studies of the properties of a semi-infinite PC in air. The proposed method also can support important information that in the supercell calculation method how large the spacing between two defect layers is appropriate when treating them as the isolated defect layers, neglecting their coupling effect.

Finally, we would indicate the deficiency of the proposed method. The proposed method may not be sufficiently efficient because we obtain all the solutions in the whole k space, including both inside and outside the first Brillouin zone (FBZ). However, only the solutions inside the FBZ are available because the solutions outside the FBZ only provide repeated information to be redundant. For example, if we use N^2 bases, there are only $2N$ available eigenfunctions, but for the 2D system, it does not cause a big problem. The examples shown in Figs. 3–5 are calculated on an AMD 1800MP computer, using MATLAB code, and employing the number of bases to be 19×19. Plotting Figs. 3 and 4 it takes about 10 min and plotting Fig. 5 takes about 9 h with the use

of 300 segments in the frequency regime. On the contrary, this method possesses several dominant advantages. First, the frequency is first given in the calculations, thus our method can powerfully deal with the systems involving the materials with frequency-dependent (or complex number, i.e., the dissipated system) permeability and permittivity in arbitrary form. The computing times of the computer in dealing with these different systems is almost the same. Second, using this method can easily analyze the properties of periodically structural samples with interfaces or surface, and the computational time is independent of the number of layers in the samples. Thus, even if the number of layers is very large, the benefit of the time saving in the computations remains unchanged. Third, the equifrequency contours are easily determined by Eqs. (4) and (5); these contours can be used in several different purposes. For instance, as a realizing tool for studying the phenomena of negative refraction, by using Eq. (8), we can calculate the density of photonic states $D(\omega)$ as

$$D(\omega) = \int_{shell} \frac{dk_{\|}}{|\nabla_{\mathbf{k}}\omega|}. \tag{9}$$

They are especially useful when we aim at evaluating the density of states in some small frequency regimes. The studies of the properties of the finite size specimens and the samples with line defects are progressing smoothly now.

We are indebted to Professor B. Y. Gu for instructing us about the investigation of Andreev reflection [19], which provides us a chance to apply the idea of the expanded basis to the derivation of Eq. (4), and also thank him for critically reading and improving this manuscript. We acknowledge Dr. P. G. Luan who let us find the possibility of more potential applications of our method. We also thank Professor A. J. Freeman for helpful suggestions in improving our manuscript. This work was supported by the National Science Council of the Republic of China under Grant No. NSC91-2112-M-009-047.

[1] C. M. Surko and P. Kolodner, Phys. Rev. Lett. **58**, 2055 (1987); S. John, *ibid.* **58**, 2486 (1987).
[2] E. Yablonovitch, T. J. Gmitter, R. D. Meade, A. M. Rappe, K. D. Brommer, and J. D. Joannopoulos, Phys. Rev. Lett. **67**, 3380 (1991).
[3] E. Yablonovitch, T. J. Gmitter, and K. M. Leung, Phys. Rev. Lett. **67**, 2295 (1991).
[4] G. Kurizki and A. Z. Genack, Phys. Rev. Lett. **61**, 2269 (1988).
[5] S. John and J. Wang, Phys. Rev. B **43**, 12772 (1991).
[6] S. L. McCall, P. M. Platzman, R. Dalichaouch, D. Smith, and S. Schultz, Phys. Rev. Lett. **67**, 2017 (1991).
[7] K. Sakoda, *Optical Properties of Photonic Crystals* (Springer-Verlag, Berlin, 2001).
[8] Z. Y. Li, B. Y. Gu, and G. Z. Yang, Phys. Rev. Lett. **81**, 2574 (1998); Eur. Phys. J. B **11**, 65 (1999).
[9] K. Sakoda, Phys. Rev. B **52**, 8992 (1995).
[10] J. B. Pendry, J. Mod. Opt. **41**, 209 (1994).
[11] B. Gralak, S. Enoch, and G. Tayeb, J. Opt. Soc. Am. A **17**, 1012 (2000).
[12] J. B. Pendry and A. MacKinnon, Phys. Rev. Lett. **69**, 2772 (1992).
[13] J. B. Pendry, J. Phys.: Condens. Matter **8**, 1085 (1996).
[14] N. Stefanou, V. Karathanos, and A. Modinos, J. Phys.: Condens. Matter **4**, 7389 (1992).
[15] V. Yannopapas, N. Stefanou, and A. Modinos, J. Phys.: Condens. Matter **9**, 10 261 (1997).
[16] N. Stefanou, V. Yannopapas, and A. Modinos, Comput. Phys. Commun. **132**, 189 (2000).
[17] K. Ohtaka, Phys. Rev. B **19**, 5057 (1979); J. Phys. C **13**, 667 (1980); A. Modinos, Physica A **141**, 575 (1987).
[18] L. C. Botten, N. A. Nicorovici, R. C. McPhedran, C. Martijn de Sterke, and A. A. Asatryan, Phys. Rev. E **64**, 046603 (2001).
[19] Y. C. Hsue, T. J. Yang, B. Y. Gu, and J. Wang, Eur. Phys. J. B **34**, 237 (2003).